JACS
JOURNAL OF THE AMERICAN CHEMICAL SOCIETY
Article
pubs.acs.org/JACS

Electronic States of the Quasilinear Molecule Propargylene (HCCCH) from Negative Ion Photoelectron Spectroscopy

David L. Osborn,*[,†,‡] Kristen M. Vogelhuber,[‡] Scott W. Wren,[‡,#] Elisa M. Miller,[‡,▽] Yu-Ju Lu,[‡] Amanda S. Case,[‡,○] Leonid Sheps,[†] Robert J. McMahon,[§] John F. Stanton,[∥] Lawrence B. Harding,[⊥] Branko Ruscic,[⊥] and W. Carl Lineberger*[,‡]

[†]Combustion Research Facility, Sandia National Laboratories, Livermore, California 94551-0969, United States
[‡]JILA and Department of Chemistry and Biochemistry, University of Colorado, Boulder, Colorado 80309-0440, United States
[§]Department of Chemistry, University of Wisconsin-Madison, Madison, Wisconsin 53706-1322, United States
[∥]Institute for Theoretical Chemistry, Department of Chemistry and Biochemistry, The University of Texas at Austin, Austin, Texas 78712, United States
[⊥]Division of Chemical Sciences and Engineering, Argonne National Laboratory, Argonne, Illinois 60439, United States

Supporting Information

ABSTRACT: We use gas-phase negative ion photoelectron spectroscopy to study the quasilinear carbene propargylene, HCCCH, and its isotopologue DCCCD. Photodetachment from $HCCCH^-$ affords the $\tilde{X}(^3B)$ ground state of HCCCH and its $\tilde{a}(^1A)$, $\tilde{b}$ (^1B), $\tilde{d}(^1A_2)$, and $\tilde{B}(^3A_2)$ excited states. Extended, negatively anharmonic vibrational progressions in the $\tilde{X}(^3B)$ ground state and the open-shell singlet $\tilde{b}$ (^1B) state arise from the change in geometry between the anion and the neutral states and complicate the assignment of the origin peak. The geometry change arising from electron photodetachment results in excitation of the ν_4 symmetric CCH bending mode, with a measured fundamental frequency of 363 ± 57 cm^{-1} in the $\tilde{X}(^3B)$ state. Our calculated harmonic frequency for this mode is 359 cm^{-1}. The Franck−Condon envelope of this progression cannot be reproduced within the harmonic approximation. The spectra of the $\tilde{a}(^1A)$, $\tilde{d}(^1A_2)$, and $\tilde{B}(^3A_2)$ states are each characterized by a short vibrational progression and a prominent origin peak, establishing that the geometries of the anion and these neutral states are similar. Through comparison of the $HCCCH^-$ and $DCCCD^-$ photoelectron spectra, we measure the electron affinity of HCCCH to be 1.156 $\pm^{0.010}_{0.095}$ eV, with a singlet−triplet splitting between the $\tilde{X}(^3B)$ and the $\tilde{a}(^1A)$ states of ΔE_{ST} = 0.500 $\pm^{0.10}_{0.01}$ eV (11.5 $\pm^{2.3}_{0.2}$ kcal/mol). Experimental term energies of the higher excited states are T_0 $[\tilde{b}(^1B)]$ = 0.94 $\pm^{0.22}_{0.20}$eV, T_0 $[\tilde{d}(^1A_2)]$ = 3.30 $\pm^{0.10}_{0.02}$eV, T_0 $[\tilde{B}(^3A_2)]$ = 3.58 $\pm^{0.10}_{0.02}$eV. The photoelectron angular distributions show significant π character in all the frontier molecular orbitals, with additional σ character in orbitals that create the $\tilde{X}(^3B)$ and $\tilde{b}(^1B)$ states upon electron detachment. These results are consistent with a quasilinear, nonplanar, doubly allylic structure of $\tilde{X}(^3B)$ HCCCH with both diradical and carbene character.

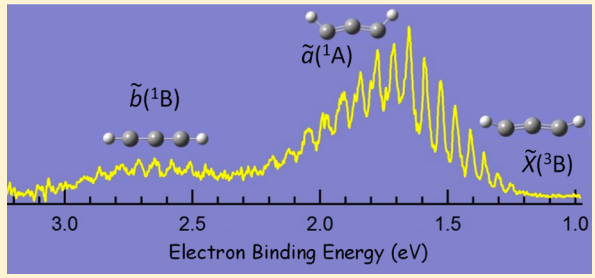

1. INTRODUCTION

Carbenes, hydrocarbons in which one carbon atom has two unshared valence electrons, are a ubiquitous and fascinating class of compounds that play central roles in organic chemistry, combustion chemistry, and astrochemistry. The simplest carbene, methylene (H_2C:), can achieve electron sufficiency (satisfied octet) only through bimolecular reactions, whereas carbenes containing two carbons, vinylidene ($H_2C{=}C$:) and ethylidene ($H_3C{-}\ddot{C}{-}H$), can achieve electron sufficiency through intramolecular rearrangement (forming $HC{\equiv}CH$ and $H_2C{=}CH_2$, respectively). The addition of a third carbon atom broadens the carbene landscape, with C_3H_2 the best prototype of this expanded complexity. Propargylene **1**, propadienylidene **2**, and cyclopropenylidene **3** represent three of the possible structures on the C_3H_2 potential energy surface (Schemes 1 and 2). In addition to many structural isomers that now become plausible, more than one carbon atom may act as the carbene center, and conjugation among π orbitals is possible. Although intramolecular rearrangements are possible,

Scheme 1. Possible Valence Bond Structures of Triplet Propargylene 1

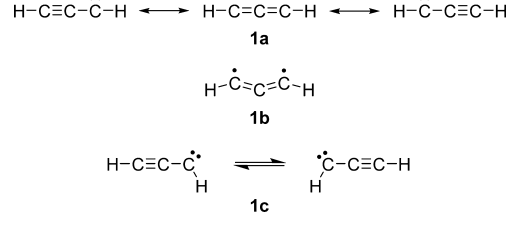

Received: April 22, 2014

   dx.doi.org/10.1021/ja5039984 | J. Am. Chem. Soc. XXXX, XXX, XXX−XXX

Scheme 2. C_3H_2 Isomers and Their Computed Relative Energies[a]

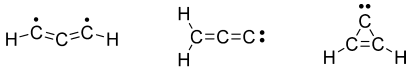

1b	2	3
12.1	*14.1*	*0.0*

[a]Energy (kcal/mol; ZPVE included). CCSD(T)/CBS, this work.

none afford a stable (isolable) species because of the high degree of unsaturation. For these reasons, the C_3H_2 system has been the subject of many investigations to determine molecular and electronic structures, both for fundamental understanding and for elucidating reaction mechanisms.

In this article, we use gas phase negative ion photoelectron spectroscopy to investigate the HCCCH isomer, known as propargylene or propynylidene, and its fully deuterated isotopologue, DCCCD. We measure the electron affinity (EA) of propargylene and observe vibrational progressions in five electronic states of this molecule. We compare these results with high-level electronic structure calculations for additional insight. Together, the photoelectron spectra, their angular dependence, and the calculations characterize the molecular structure of the propargylene anion, the quasilinear ground state and four excited states of neutral HCCCH.

2. BACKGROUND

Propargylene **1** may be considered the simplest acetylenic carbene, although the extensive electronic delocalization also confers significant diradical character. Observation of the triplet electron paramagnetic resonance (EPR) spectrum of propargylene at 10 K establishes that the triplet state is the ground electronic state, as predicted by theory.[1] The structure of triplet propargylene **1** has been variously considered to be linear (**1a**, $D_{\infty h}$), bent (**1c**, C_s), or doubly bent (**1b**, C_2) (Scheme 1).

Recent experimental and theoretical studies appear to converge to an interpretation in terms of a C_2 structure (**1b**) that is quasilinear (i.e., a bent equilibrium structure in which the barrier to linearity lies below the zero-point energy level).[1] Singlet propadienylidene **2** (the simplest vinylidene carbene) lies close in energy to propargylene **1**, both of which lie higher in energy than singlet cyclopropenylidene **3** (the smallest aromatic carbene) (Scheme 2). These C_3H_2 isomers undergo a number of isomerization and automerization processes under both thermal and photochemical conditions.[2,3]

The lowest energy C_3H_2 isomer is cyclopropenylidene (c-C_3H_2) **3**, one of the most abundant organic compounds in the interstellar medium (ISM),[4] as detected by radio astronomy.[5,6] In the laboratory, c-C_3H_2 (**3**) was first studied using matrix isolation infrared (IR) spectroscopy[7] and later via rotational spectroscopy,[5,8] photoelectron spectroscopy,[9] and electronic absorption spectroscopy.[3] Cyclopropenylidene **3** has a singlet ground state, a large dipole moment (3.3−3.4 D),[10,11] and a rigid structure in C_{2v} symmetry.[8]

Propadienylidene **2** is also abundant in the ISM. It has been detected by radio astronomy in both dense clouds (IRC+10216 and TMC-1)[12,13] and the diffuse ISM.[14] The electronic absorption spectrum of propadienylidene **2** exhibits two features that are coincident in position and absorption profile with two of the diffuse interstellar bands (DIBs).[15] This astronomical assignment was controversial and has been disputed.[16,17] Microwave spectroscopy,[18−20] in combination with theory,[21] indicates the equilibrium geometry of H_2CCC is a rigid, near prolate top in C_{2v} symmetry, with a singlet ground state and a large dipole moment (4.1 D). Propadienylidene has been studied extensively in the laboratory using IR spectroscopy,[2,3,22] photoelectron spectroscopy,[9] negative-ion photoelectron spectroscopy,[23−25] and electronic absorption spectroscopy.[26−30]

Returning to the focus of this study, propargylene **1** (HCCCH) was first observed by Bernheim, Skell, and coworkers in 1965 by EPR spectroscopy following photolysis of diazopropyne in a solid matrix at 77 K.[31] These investigators assigned a triplet ground state to HCCCH with a linear geometry. Vibrational fundamentals of HCCCH have been measured via matrix isolation IR spectroscopy.[32−34] McMahon and co-workers, in a series of site-specific ^{13}C and ^{2}H isotopic labeling experiments, used matrix isolation IR and EPR spectroscopy to obtain substantial evidence in support of a C_2-symmetric, but quasilinear, structure (**1b**) for the triplet ground state of HCCCH.[1−3] Rather than attempting to categorize triplet propargylene **1** as a carbene vs a diradical, analysis using natural resonance theory suggests that triplet HCCCH is best viewed as a significant admixture of both.[1,35]

Isomers of C_3H_2, particularly HCCCH, are important in combustion chemistry and have been implicated in the formation of polycyclic aromatic hydrocarbons and soot.[36,37] C_3H_2 has been detected in C_2H_4/O_2 flames[38] and identified as an intermediate in the formation of C_2H from $C_2H_2/O/H$ flames.[39] In a photoionization efficiency study of C_3H_2 in a rich cyclopentene flame, Taatjes et al. measured the ionization energy (IE) of ^{3}HCCCH and found evidence for the presence of both HCCCH and cyclopropenylidene in this flame.[40] C_3H_2 isomers have been observed as products of the crossed molecular beam reaction of CH and C_2H_2.[41] Ab initio calculations and RRKM analysis show that ^{3}HCCCH is a primary product of the reaction of C_2H_2 with CH and other hydrocarbons.[42−45] In contrast, an experimental study of the CH + C_2H_2 reaction detects c-C_3H_2 as the main product of this reaction, using VUV photoionization with time-resolved mass spectrometry.[46] Recently, the adiabatic IE of HCCCH has been measured.[47]

In addition to the relevance of propargylene in astrochemistry, combustion chemistry, and its fundamental importance as the smallest "acetylenic carbene," substituted propargylene derivatives are used as ligands in organometallic chemistry,[48,49] and their interesting reactivity has been applied to organic synthesis.[50,51] The spectroscopic signatures of diradical character in HCCCH notwithstanding, the general reactivity patterns exhibited by propargylene derivatives are characteristic of an acetylenic carbene.[1]

The technique of gas phase negative ion photoelectron spectrometry is a powerful complement to the matrix IR and EPR approaches. Negative ion photoelectron spectroscopy can be used to measure the EA and singlet−triplet splitting (ΔE_{ST}) of HCCCH, both fundamentally important values. The nuclear and electronic configuration of the precursor anion provides a reference to which all neutral electronic states may be compared. The angular distribution of the electrons relative to the electric field of the detachment laser provides important clues to the nature of the electronic states and hence the molecular structure of HCCCH. Finally, gas phase negative ion photoelectron spectroscopy accesses higher lying vibrational and electronic states of the isolated molecule, providing valuable information on the shape of the potential energy

dx.doi.org/10.1021/ja5039984 | J. Am. Chem. Soc. XXXX, XXX, XXX−XXX

surfaces without the potential perturbations of a matrix environment.

3. EXPERIMENTAL METHODS

The negative ion photoelectron spectrometer (NIPES) used in this experiment has been described in detail elsewhere.[52−54] Briefly, photoelectron spectra of $HCCCH^-$ were acquired using Argon ion laser excitation at 3.40814 eV and a hemispherical electron energy analyzer that provides constant energy resolution of 11 meV irrespective of the electron kinetic energy. Additional details are provided as Supporting Information. Negative ions are formed in a flowing afterglow ion source. A microwave discharge containing trace amounts of O_2 gas in He buffer gas (~0.4 Torr) generates atomic oxygen radical anion, O^-. Propyne ($H_3CC{\equiv}CH$) is added downstream of O^- to generate both propargylenide ($HCCCH^-$) and propadienylidenide (H_2CCC^-) anions (m/z = 38):

$$O^- + H_3C{-}C{\equiv}CH \rightarrow HC{=}C{=}CH^- + H_2O$$
$$O^- + H_3C{-}C{\equiv}CH \rightarrow H_2C{=}C{=}C^- + H_2O$$
$$O^- + H_2C{=}C{=}CH_2 \rightarrow H_2C{=}C{=}C^- + H_2O \quad (1)$$

In a separate experiment, reaction of O^- with allene ($H_2C{=}C{=}CH_2$) generates predominantly propadienylidene (H_2CCC^-).[23,24] Dawson et al. first observed these different yields of $C_3H_2^-$ isomers formed from propyne vs allene from reactivity of the anions with methyl formate.[55] Subtraction of the latter spectrum (appropriately scaled) from the former yields the photoelectron spectrum of the propargylenide isomer. Similarly, propyne-d_4 ($D_3CC{\equiv}CD$) and allene-d_4 ($D_2C{=}C{=}CD_2$) are used to produce $DCCCD^-$ and D_2CCC^-. Collisions with He buffer gas cool the ions to approximately 300 K. The flow tube can be further cooled with a liquid nitrogen jacket to obtain a "cold spectrum" of ions with a temperature near 150 K. In the case of propargylene, vibrational cooling of the anions with liquid nitrogen dramatically improves our ability to resolve vibrational structure; thus, with one exception, all photoelectron spectra shown in this work were collected at ~150 K.

In addition to formation of $C_3H_2^-$ isomers, we also observe formation of the allenyl anion ($H_2C{=}C{=}CH^-$) and the 1-propynyl anion ($H_3C{-}C{\equiv}C^-$) at m/z = 39 when propyne reacts with O^-. Optimal production of $C_3H_2^-$ isomers occurs with low concentrations of propyne such that O^- ions are not completely titrated. Further details of the ion−molecule chemistry are provided in the Supporting Information.

We performed additional, complementary experiments using a negative ion velocity-map imaging[56,57] (VMI) photoelectron spectrometer.[58] Although this apparatus has somewhat reduced electron kinetic energy resolution compared to the NIPES apparatus, it uses a pulsed, tunable photodetachment laser that provides access to higher-lying states of HCCCH. Details of this apparatus are given in the Supporting Information.

4. THEORETICAL METHODS

We use two electronic structure methods to calculate geometries, harmonic vibrational frequencies, and energies extrapolated to the complete basis set limit for anions and neutrals. The lowest electronic state of each symmetry is calculated using coupled cluster (CCSD(T)) theory. Geometries and harmonic frequencies are calculated at the CCSD(T)/aug-cc-pVTZ level, with energies calculated using analogous 4Z and 5Z basis sets. The energy is extrapolated to the complete basis set limit $E(\infty)$ by fitting the energies $E(L)$, calculated using basis sets with maximum angular momenta L = 3, 4, and 5, to the equation $E(L) = E(\infty) + B(L+1)^{-4}$. The resulting energies of the three C_3H_2 isomers in Scheme 2 are in good agreement with the recent high-level calculations of Aguilera-Iparraguirre et al.[59] Because CCSD(T) can be difficult to apply to certain excited states of radicals, we have also calculated all electronic states using multireference configuration interaction (MRCI), with geometries and frequencies at the (6e,6o)-CAS+1+2+QC/aug-cc-pVTZ level of theory, and energies up to the aug-cc-pVQZ basis set extrapolated to the complete basis set limit. We utilized the Gaussian09 package[60] with unrestricted wave functions to calculate the electronic states of the anions and the ground state of the neutral. For all other electronic states, and all MRCI calculations, we employed restricted wave functions using the MolPro package.[61] The active space can be described as follows: if one considers HCCCH as a linear molecule, with its symmetry axis along the z-axis, the 6-electron/6-orbital active space is composed of three p_x and three p_y atomic carbon orbitals that together form three π_x and three π_y molecular orbitals, with zero, one, and two nodes perpendicular to the z-axis, respectively.

We benchmark the calculations to experimental adiabatic detachment energies (ADEs) of the 21-electron anions H_2CCC^-, $HCCN^-$,[62]

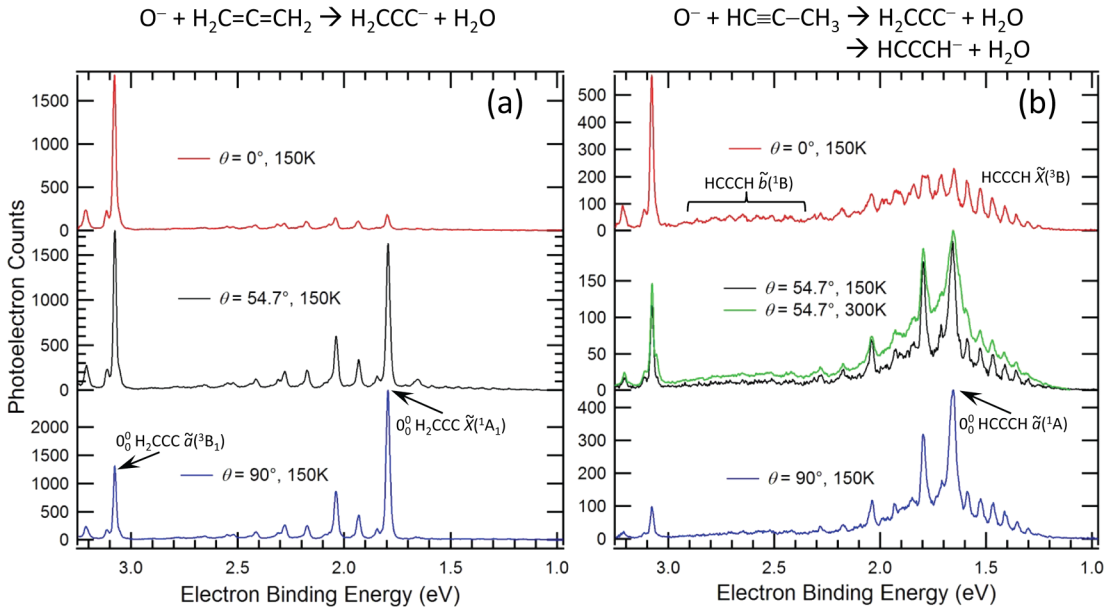

Figure 1. Photoelectron spectra of the product anions from (a) O^- + allene and (b) O^- + propyne. θ is the angle between the electric field polarization vector and the axis of electron detection.

dx.doi.org/10.1021/ja5039984 | J. Am. Chem. Soc. XXXX, XXX, XXX−XXX

and NCN^-[63] (the latter two being isoelectronic with $HCCCH^-$). The CCSD(T)/CBS results differ at most by 0.019 eV from experiment, even when excited electronic states of the neutrals are included. The results show that the MRCI/CBS calculations provide detachment energies that are systematically lower by ~0.13 eV compared to the experimentally validated CCSD(T) calculations. We assume that this offset is transferable to all electronic states of neutral HCCCH and use it to correct the MRCI energies before comparison with experiment.

5. RESULTS

5.1. Isomer-Specific Chemistry. When O^- reacts with a hydrocarbon, it usually removes a hydrogen atom and a proton, forming neutral H_2O and a hydrocarbon anion. In the case of the O^- + C_3H_4 reaction, the isomer distribution of the $C_3H_2^-$ anion depends on the isomeric form of the C_3H_4 reactant. Using the NIPES apparatus, the O^- + allene ($H_2C{=}C{=}CH_2$) reaction yields the relatively simple photoelectron spectra in Figure 1a, which arise almost exclusively from electron detachment of the propadienylidenide anion, H_2CCC^-, in agreement with previous results.[24,25] By contrast, when O^- reacts with propyne ($H_3CC{\equiv}CH$), the spectra in Figure 1b show many new features in addition to all the peaks observed in Figure 1a. This observation provides strong evidence that the reaction of O^- with propyne forms at least one additional isomer of $C_3H_2^-$ in significant yield. We will show below that all of the new features in Figure 1b can be conclusively assigned to transitions from the propargylenide anion, $HCCCH^-$. We note that the NIPES spectrum of Robinson et al.[24] resulting from the O^- + allene reaction contains a weak unassigned feature at ~1.66 eV binding energy, corresponding in energy to the strongest feature in our $HCCCH^-$ spectra, and is an almost certain indication of a minor $HCCCH^-$ component in their $C_3H_2^-$ anion beam.

A close inspection of peak widths as a function of anion temperature in the θ = 54.7° "magic angle" spectra in Figure 1b provides further evidence for the presence of two different isomers of $C_3H_2^-$. Decreasing the flow tube temperature from 300 to 150 K, the peak at eBE = 1.796 eV, assigned to the origin of H_2CCC $\tilde{X}(^1A_1)$, shows only modest narrowing, in contrast to the dramatic narrowing of the peak at 1.656 eV. This behavior is further evidence that the latter feature is not a part of the well-known photoelectron spectrum of the rigid H_2CCC^-, but rather it arises from an isomer with multiple low frequency modes that are thermally populated and active in photodetachment. Such behavior is consistent with this peak arising from photodetachment of $HCCCH^-$. Corresponding photoelectron spectra from the reactions of O^- with allene-d_4 and propyne-d_4 are shown in Figure S1 of the Supporting Information.

Figure 2 shows spectra from the VMI photoelectron spectrometer, which can utilize higher photon energies than available with the NIPES spectrometer, allowing access to higher-lying electronic states of HCCCH. The right portion of Figure 2, acquired at a photon energy of 2.352 eV, provides a direct comparison with the NIPES spectra in Figure 1. Although the anion source in the VMI instrument is different from that in the NIPES instrument, comparing features from 1.4 to 2.1 eV binding energy between the two instruments shows the same isomer-specific chemistry in both sources. We therefore conclude, at all binding energies, that the black spectra (allene reactant) in Figure 2 arise primarily from detachment of H_2CCC^-, whereas features in the red spectra (propyne reactant) that were not present in the black spectra

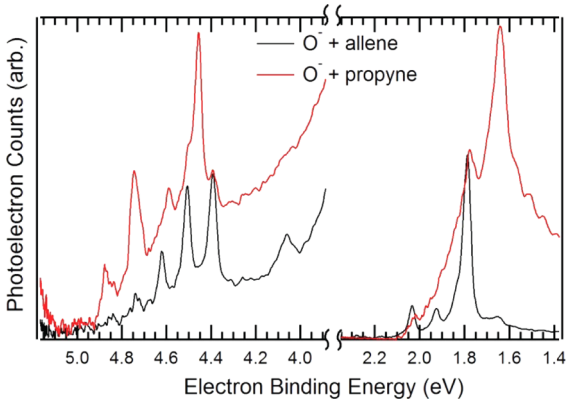

Figure 2. Photoelectron spectra of the product anions from O^- + allene (black), and O^- + propyne (red) acquired with the velocity-map imaging photoelectron spectrometer. Spectra on the right side were acquired with $h\nu$ = 2.352 eV, and on the left side with $h\nu$ = 5.158 eV.

arise from $HCCCH^-$. Using a higher photon energy of 5.158 eV, we observe the photoelectron spectra in the left portion of Figure 2, which could not be acquired on the NIPES instrument. We attribute the peaks in the red spectrum (propyne reactant) that are not present in the black spectrum (allene reactant) to higher electronic states of HCCCH.

5.2. Photoelectron Angular Distributions. Figures 1 and S1 show the change in peak intensities with respect to the angle between the electric field vector of the detachment laser and the axis of electron collection. The angular distribution of photoelectrons enables two aspects of our analysis. First, in the absence of strong vibronic coupling effects, the groups of vibrational peaks arising from one electronic state of the neutral generally have a distinct angular distribution, allowing a purely experimental method for distinguishing electronic states of the neutral even if their spectra overlap in electron binding energy. Second, because the reaction of O^- with allene happens to produce mostly H_2CCC^-, whereas the reaction with propyne shows contributions from both H_2CCC^- and $HCCCH^-$, we can subtract the O^- + allene spectra from the O^- + propyne spectra to isolate the contributions of $HCCCH^-$.

Because some electronic states of H_2CCC and HCCCH produce overlapping photoelectron spectra, we must first scale the allene-derived spectra to the propyne-derived spectra using a peak of H_2CCC that does not overlap any peaks arising from HCCCH. This method ensures complete subtraction of H_2CCC contributions even at electron binding energies where the isomers' spectra overlap. The relative spectral intensities in Figure 1a and b are identical from eBE = 3.0–3.25 eV, implying that only H_2CCC contributes in this region. The strong peak at eBE = 3.076 eV was assigned to the origin transition of H_2CCC $\tilde{a}(^3B_1)$ by Robinson et al.,[24] and we use its angle-dependent intensity to scale the spectra in Figure 1a to corresponding spectra in Figure 1b in order to quantitatively subtract contributions of H_2CCC from the propyne-derived spectra. The capability of the NIPES spectrometer to provide photoelectron spectra over wide eBE ranges (>2 eV) with fixed excitation energy and constant electron collection efficiency is critical to this isomer separation approach.

Figure S2b in the Supporting Information shows the differential detachment cross sections obtained from product anions of the O^- + propyne reaction in 150 meV-wide windows centered at either eBE = 3.076 eV (the origin of the H_2CCC $\tilde{a}(^3B_1)$ state) or eBE = 1.671 eV, where the signal arises

dx.doi.org/10.1021/ja5039984 | J. Am. Chem. Soc. XXXX, XXX, XXX–XXX

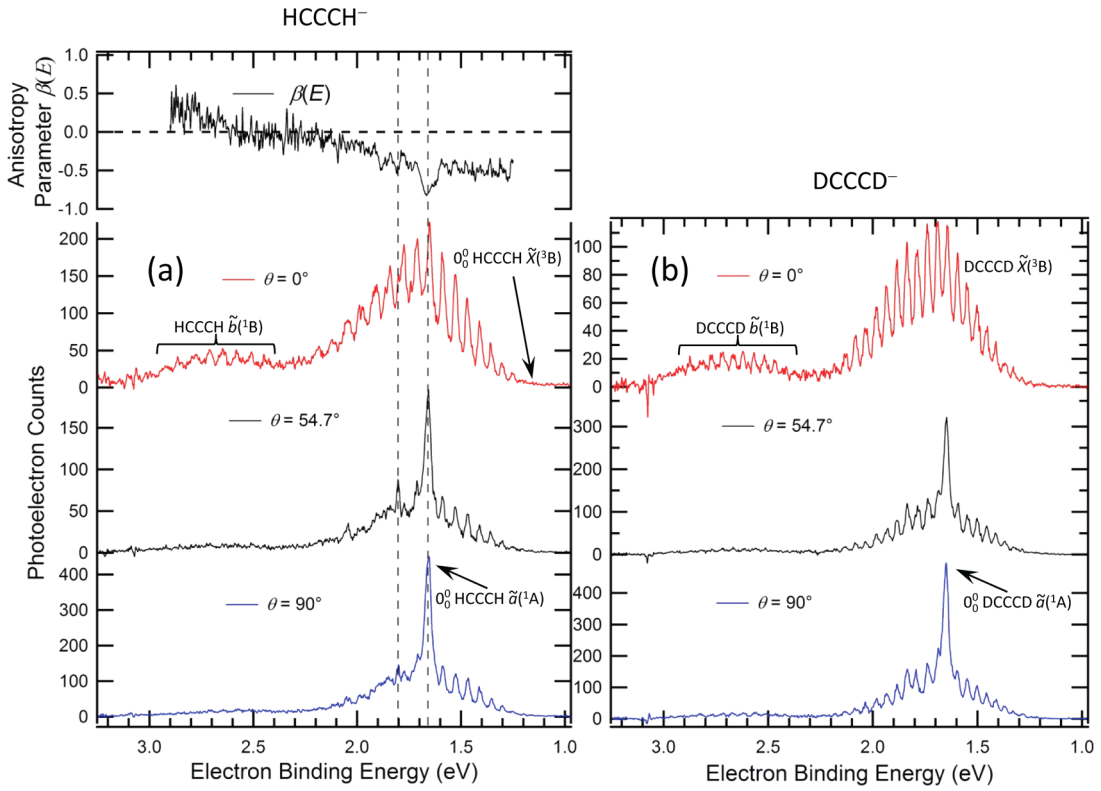

Figure 3. Photoelectron spectra of (a) $HCCCH^-$, and (b) $DCCCD^-$ with contributions from H_2CCC^- and D_2CCC^- subtracted. θ is the angle between the electric field polarization vector and the axis of electron detection. Ion temperature is ~150 K. The artifacts at 3.076 eV arise from imperfect subtraction of the propadienylidene contributions. The energy-resolved anisotropy parameter $\beta(E)$ is shown for $HCCCH^-$. The vertical dashed lines show transitions to the $\tilde{a}(^1A)$ electronic state of HCCCH.

primarily from the $\tilde{a}(^1A)$ state of HCCCH. We extract anisotropy parameters $\beta[H_2CCC\ \tilde{a}(^3B_1)] = +0.60 \pm 0.04$ and $\beta[HCCCH\ \tilde{a}(^1A)] = -0.69 \pm 0.02$ by fitting eq S1 (Supporting Information) to the data in Figure S2b. Such measurements, at many different electron ejection angles, are the most robust method for obtaining β but are too time-consuming to acquire the complete energy dependence of the anisotropy parameter $\beta(E)$.

Figure S3a shows photoelectron spectra from the O^- + propyne reaction normalized to the differential cross section for electron detachment from H_2CCC^- at 3.076 eV. These three spectra allow a three-point fit to eq S1 at each electron binding energy, providing $\beta(E)$, which is plotted above the spectra.

5.3. Photoelectron Spectra of $HCCCH^-$ and $DCCCD^-$. Subtracting the contributions of propadienylidene from the O^- + propyne and O^- + propyne-d_4 data provides the photoelectron spectra that arise from $HCCCH^-$ and $DCCCD^-$ in Figure 3a and b. (We note that Ikuta[64] finds no bound states in his calculations of the cyclopropenylidene anion. None of our results contradict this conclusion.) The energy-dependent anisotropy parameter, $\beta(E)$, is also shown in Figure 3 and is only available for the HCCCH isotopologue due to the expense of the deuterated sample. The same photoelectron spectra for HCCCH can be seen in Figure S3b, normalized to the differential cross section. This presentation of the data emphasizes that at all but the highest electron binding energies, the detachment cross section of $HCCCH^-$ is largest at $\theta = 90°$, i.e., $\beta(E) < 0$ for eBE < 2.6 eV. Such negative values correspond to detachment from a p orbital in an atomic anion, resulting in s and d partial waves of the outgoing electron. A similar analysis is much more complicated in the lower symmetry of a polyatomic molecule, but negative anisotropy parameters generally correspond to detachment from a π orbital, whereas positive values are consistent with detachment from orbitals with σ character. In addition, the abrupt changes in β as a function of binding energy (e.g., at 1.803 vs 1.773 eV) are evidence that multiple electronic states of neutral HCCCH contribute to the spectra for eBE > 1.65 eV.

The photoelectron angular distributions shown in Figure 3a provide qualitative inferences concerning the nature of the electronic states of HCCCH that are populated following electron photodetachment from the anion. The red spectrum at $\theta = 0°$ shows a long progression with a smooth envelope apparently beginning at 1.249 eV, reaching a maximum near 1.7 eV, and tapering back to baseline at ~2.3 eV. This progression is dwarfed in the black magic angle spectrum by a strong peak at 1.656 eV. The anisotropy parameter has an average value of −0.45 from 1.25−1.59 eV but becomes more energy dependent for eBE ≥ 1.65 eV. These observations are consistent with the long progression being associated with a $\tilde{X}(^3B)$ ground electronic state of HCCCH, and the sharp peak at 1.656 eV with the origin of the first excited state $\tilde{a}(^1A)$. The observed Franck−Condon profiles show that the ground state neutral geometry is quite different from the anion, whereas the geometry of the $\tilde{a}(^1A)$ state is similar to the anion. The term symbol assignments will be justified in section 6.1, and the experimental determination of the $\tilde{X}(^3B)$ origin energy in section 5.4. Finally, we assign a third electronic state, the $\tilde{b}(^1B)$ state, to the series of peaks from ~2.4−2.95 eV, which are most prominent in the $\theta = 0°$ spectra, and for which a large geometry change from the anion seems clear due to the long vibrational progression. This progression shows an energy dependent

dx.doi.org/10.1021/ja5039984 | J. Am. Chem. Soc. XXXX, XXX, XXX−XXX

anisotropy parameter that rises from −0.1 to +0.2 with increasing eBE. On the basis of the intensities of the features in this progression there is little hope of locating the origin transition of the $\tilde{b}(^1B)$ state, but we assign a band envelope maximum of 2.65 ± 0.02 eV, which agrees reasonably well with the calculated VDE of 2.75 eV (section 5.5). The corresponding photoelectron spectra of $DCCCD^-$ in Figure 3b support these assignments of electronic states.

It is more difficult to draw conclusions purely from experiment about the spectra in Figure 2, which probe higher-lying electronic states of HCCCH. Focusing on the peaks in the red spectra (propyne-derived) that are not present in the black spectra (allene-derived), there appear to be four peaks that arise from HCCCH at eBE = 4.454, 4.590, 4.738, and 4.869 eV.

5.4. Experimental Assignment of the HCCCH $\tilde{X}(^3B)$ Origin. It is challenging to experimentally assign the origin of an electronic transition with a large geometry change from anion to neutral because the small Franck−Condon factor of the origin transition may make it difficult or impossible to observe above the noise.[65] Figure 4 shows photoelectron spectra of $HCCCH^-$ and $DCCCD^-$ in the region of the expected $\tilde{X}(^3B)$ origin transition, where a shorter scan range enables greater signal averaging. Cooling the anions to ∼150 K should diminish the intensity of hot band transitions from vibrationally excited anions. Peak positions for the two isotopomers, taken from Figures 3 and 4, are shown in Table 1. Starting from the peaks with the lowest observed eBE in both isotopologs, and despite potential unresolved structure in the peak shapes, the peak spacings increase smoothly, indicating significant anharmonicity. The progression is well fit by a single anharmonicity constant (see Supporting Information), with no abrupt changes in peak spacing that would indicate the presence of hot bands. The lowest binding energy observed is the peak at 1.156 eV in the HCCCH spectrum. However, the intensity of the vibrations in this progression drops by a factor of ∼2 from one peak to the next. If there were another peak beyond the 1.156 eV peak, it would have escaped detection. Therefore, this analysis only concludes that the origin of the HCCCH progression must be at a binding energy of 1.156 eV (the first observed peak) or lower, and we can only claim that EA(HCCCH) ≤ 1.156 eV.

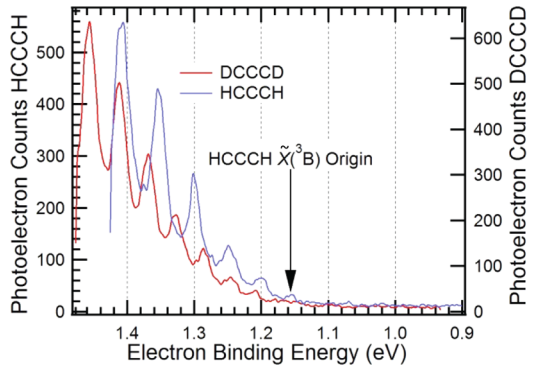

Figure 4. Photoelectron spectra of $HCCCH^-$ and $DCCCD^-$ with θ = 90° laser polarization and anion temperature of ∼150 K.

In an effort to assign the origin transition in experimental spectra with long vibrational progressions, such as observed here, Robinson et al.[24] used a simple isotopic substitution method. They compared peaks in a long vibrational progression from allenyl (H_2CCCH^-) and allenyl-d_3 (D_2CCCD^-) anions to determine the EA of the propargyl radical (H_2CCCH). They did so by recognizing that the origin transition energy of nondeuterated and fully deuterated species will occur at the same electron binding energy, apart from a small difference due to differential zero point energy (ZPE) changes upon deuteration. As one example of this change, photoelectron spectra of d_0 and d_3 methoxide anions show strong, well-defined origin transitions, with EA(CH_3O) = 1.5690 ± 0.0019 eV, but EA(CD_3O) = 1.5546 ± 0.0019 eV, a difference of over 14 meV.[66] In addition to this example, per-deuterated and undeuterated EAs are experimentally known for OH, HO_2, CH_3, CCH, CH_2, C_3H, C_3H_5, and $CH_2C(CH_3)CH_2$. In all cases but one, the per-deuterated EA is less than the undeuterated EA, by up to 17 meV.

As stated above, we observe an $HCCCH^-$ peak at 1.156 eV that we believe is not a hot band and claim it to represent an upper bound for EA(HCCCH). Unfortunately, there are no definitive $DCCCD^-$ peaks below 1.208 eV, due to noise limitations. More sophisticated extrapolations (see Supporting Information) of unobserved peaks suggest a possible origin as low as 1.07 eV eBE, an assignment that would minimize the difference between EA(HCCCH) and EA(DCCCD). However, measured EAs of undeuterated vs per-deuterated molecules differ by up to 17 meV. Furthermore, calculated EAs tend to approach the true value from below because each improvement to the basis set stabilizes the diffuse anion more than the compact neutral. Comparing with our highest level CCSD(T)/CBS calculated values of EA(HCCCH) = 1.146 eV and EA(DCCCD) = 1.144 eV, we conclude that it is very unlikely that the origin lies below 1.07 eV. For these reasons, we assign EA(HCCCH) = $1.156 \pm {}^{0.010}_{0.095}$ eV. On the basis of our assignment, the singlet−triplet splitting between the $\tilde{a}(^1A)$ and the $\tilde{X}(^3B)$ states of HCCCH is determined to be ΔE_{ST} = 1.656−1.156 = $0.500 \pm {}^{0.10}_{0.01}$ eV.

5.5. Theoretical Results. We start our discussion of the electronic structure of neutral HCCCH by considering a hypothetical linear structure with atoms on the z axis. The first six electrons will occupy nonbonding C(1s) core orbitals. The next eight electrons form four σ bonds between the five atoms. The remaining six electrons fill π orbitals in the x and y planes that have 0 or 1 node perpendicular to the z axis. One expects a $\pi_u^4\pi_g^2$ orbital occupancy for the ground state, implying a $^3\Sigma_g^-$ ground state with a low-lying $^1\Delta$ excited state. Higher lying neutral states would result from π_u to π_g excitations.

The ground state of HCCCH is computed to have C_2 symmetry.[1,59] The distortion from linearity transforms the ground state from $^3\Sigma_g^-$ to ^3B and splits the degenerate $^1\Delta$ state into a Renner−Teller pair of states having symmetries ^1A and ^1B in the C_2 point group (Figure S4, Table 2). Although there has been some work on the Renner−Teller effect in five-atom molecules,[67] an analysis of this effect in HCCCH is beyond the scope of this paper.

A similar situation pertains to the propargylenide anion ($HCCCH^-$). A hypothetical linear anion with seven π electrons is expected to have a $^2\Pi_g$ ground state, with an orbital occupancy of $\pi_u^4\pi_g^3$. Calculations predict the propargylenide anion to have a nearly planar, nonlinear geometry with C_2 symmetry. The distortion from linearity again results from the Renner−Teller interaction, splitting the degenerate $^2\Pi_g$ electronic state into a nondegenerate $\tilde{X}(^2B)$ and $\tilde{A}(^2A)$ pair of states through interaction with one (or more) of the three doubly degenerate bending modes of linear $HCCCH^-$. The

dx.doi.org/10.1021/ja5039984 | J. Am. Chem. Soc. XXXX, XXX, XXX−XXX

Table 1. Peak Assignments, Electron Binding Energies, Adiabatic Detachment Energies, and Term Energies Determined from the Photoelectron Spectra of $HCCCH^-$ and $DCCCD^-$[a]

		$HCCCH^-$			$DCCCD^-$
electronic state	mode assignment	electron binding energy	adiabatic detachment	term energy	electron binding energy
$\tilde{X}(^3B)$	$\nu_4 = 0$	1.156(5)	$1.156 \pm {}^{0.010}_{0.095}$	0.0	
	$\nu_4 = 1$	1.201(5)			
	$\nu_4 = 2$	1.249(5)			1.208(5)
	$\nu_4 = 3$	1.300(5)			1.246(5)
	$\nu_4 = 4$	1.353(5)			1.286(5)
	$\nu_4 = 5$	1.410(5)			1.327(5)
	$\nu_4 = 6$	1.467(5)			1.368(5)
	$\nu_4 = 7$	1.526(5)			1.412(5)
	$\nu_4 = 8$	1.588(5)			1.456(5)
	$\nu_4 = 9$				1.502(5)
	$\nu_4 = 10$				1.549(5)
	$\nu_4 = 11$				1.599(5)
$\tilde{a}(^1A)$	$\nu_2 = 0$	1.656(5)	1.656 ± 0.005	$0.500 \pm {}^{0.10}_{0.01}$	
	$\nu_2 = 1$	1.803(5)			
$\tilde{b}(^1B)$			2.1 ± 0.2	$0.94 \pm {}^{0.22}_{0.2}$	
$\tilde{d}(^1A_2)$		4.454(20)	4.454 ± 0.020	$3.30 \pm {}^{0.10}_{0.02}$	
		4.590(20)			
$\tilde{B}(^3A_2)$		4.738(20)	4.738 ± 0.020	$3.58 \pm {}^{0.10}_{0.02}$	
		4.869(20)			

[a]All energies are in eV.

Table 2. Geometric Parameters and Detachment Energies of 21-Electron Anions and Their Corresponding Neutrals

				detachment energy (eV)			term energy[f] (eV)
				CCSD(T)/CBS	MRCI/CBS	experiment	experiment
species	state	∠CCC (deg)	∠HCC (deg)	adiabatic[a] (vertical)	adiabatic (vertical)	adiabatic (band max.)	
$HCCCH^-$	$\tilde{X}(^2B)$	179	126	0.00 (0.00)	0.00 (0.00)		
	$\tilde{A}(^2A)$	163	123	0.026	0.014 (1.23)		
HCCCH	$\tilde{X}(^3B)$	173	160	1.146 (1.772)	1.03[a] (1.62)	$1.156 \pm {}^{0.010}_{0.095}$	0.0
				(1.696)[e]		(1.71 ± 0.02)	
	$\tilde{a}(^1A)$ (^1A_g) *trans* min.	180	129		1.48[a] (1.49)	1.656 ± 0.005	$0.500 \pm {}^{0.10}_{0.01}$
	$\tilde{a}(^1A)$ ($^1A_1$) *cis* min.	162	128	(1.66)	1.49[a] (1.49)		
	$\tilde{b}(^1B)$ ($^1\Delta$)	180	180		1.82[a] (2.62)	2.1 ± 0.2	$0.94 \pm {}^{0.22}_{0.20}$
						(2.65 ± 0.02)	
	$\tilde{c}(^1A)$ ($^1\Sigma^+$)	180	180		2.48[a] (4.23)		
	$\tilde{A}(^3B)$ ($^3B_2$)	108	131		4.26[a] (4.67)		
	$\tilde{d}(^1A)$ ($^1A_2$)	160	135		4.29[b] (4.34)	4.454 ± 0.02	$3.30 \pm {}^{0.10}_{0.02}$
	$\tilde{B}(^3A)$ ($^3A_2$)	180	128	(4.79)	4.36[b] (4.38)	4.738 ± 0.02	$3.58 \pm {}^{0.10}_{0.02}$
H_2CCC	$\tilde{X}(^1A_1)$			1.80 (1.83)	1.62[a] (1.65)	1.793 ± 0.005	0.0
	$\tilde{a}(^3B_1)$			3.08 (3.16)	2.95[a] (3.02)	3.076 ± 0.005	1.283 ± 0.007
HCCN	$\tilde{X}(^3A'')$			2.02 (2.46)	1.89[a] (2.34)	2.001[c] ± 0.015	0.0
	$\tilde{a}(^1A')$			2.521 (2.533)	2.53 (2.55)	2.511[c] ± 0.004	0.510 ± 0.016
NCN	$\tilde{X}(^3\Sigma_g^-)$			2.47 (2.51)	2.36[a] (2.40)	2.481[d] ± 0.008	0.0
	$\tilde{a}(^1\Delta_g)$				(3.34)	3.491[d] ± 0.013	1.007 ± 0.015
	$\tilde{b}(^1\Sigma_g^-)$				(3.90)	4.110[d] ± 0.013	1.629 ± 0.015

[a]Includes zero point energy. [b]Does not include zero point energy. [c]Negative ion photoelectron spectroscopy.[62] [d]Negative ion photoelectron spectroscopy.[63] [e]Vertical detachment energy from the $\tilde{A}(^2A)$ anion. [f]Term energy for ã state corresponds to lowest-energy singlet-triplet gap.

$\tilde{A}(^2A)$ excited state of $HCCCH^-$ is calculated to have a *cis*-bent geometry and to lie only 0.6 kcal/mol (26 meV) above the *trans*-bent $\tilde{X}(^2B)$ ground state (Figure S4, Table 2). Given this small term energy, and assuming Boltzmann equilibrium in the 150 K flowing afterglow anion beam, the $\tilde{X}(^2B)$ ground state would comprise 86% of the population, with 14% in the electronically excited $\tilde{A}(^2A)$ state. Assigning an optimistic uncertainty of ±0.5 kcal/mol (22 meV) to the calculated energies of the anions, we conclude that both anion states could be present at similar populations in the anion beam, and our treatment below considers both anion states. Note that the anion structures in Figure S4 are both nearly planar, but the C_2 symmetry axis in the $\tilde{X}(^2B)$ state is perpendicular to the plane that nearly contains the five atoms, whereas in the $\tilde{A}(^2A)$ state the C_2 axis lies in the plane that nearly contains the atoms. Although these structures are nearly C_{2h} and C_{2v}, in the discussion that follows it is convenient to refer to nearly planar structures as simply planar, and we label the $\tilde{X}(^2B)$ state as *transoid*, and the $\tilde{A}(^2A)$ state as *cisoid*. Similarly for the neutral geometries, the atoms deviate only slightly from a planar

dx.doi.org/10.1021/ja5039984 | J. Am. Chem. Soc. XXXX, XXX, XXX−XXX

geometry, and the designations "in-plane" and "out-of-plane", while not strictly accurate, are approximately correct and descriptive.

ADEs and vertical detachment energies (VDEs) resulting from our CCSD(T) and MRCI calculations are shown in Table 2, along with comparisons to our experimentally derived transition energies. All the excited electronic states of HCCCH shown are accessible by removal of a single electron from the $\tilde{X}(^2B)$ or $\tilde{A}(^2A)$ anion states. The Supporting Information provides a discussion of the expected energy ordering of the electronic states based on molecular orbital arguments.

In the ∠CCC coordinate, the geometry change from either anion, $\tilde{X}(^2B)$ or $\tilde{A}(^2A)$, is only −6° or +8° upon detachment to the neutral (Figure S5a). In the ∠CCH coordinate, however, the change is pronounced. The anion states are strongly bent, with moderate barriers to linearity (5122 and 4912 cm^{-1}, respectively). Upon detachment, the ∠CCH in the neutral increases by ∼35°, and the barrier to linearity is quite low and flat, with less than a 240 cm^{-1} energy variation over a ± 30° range around linearity. Together, the large change in ∠CCH and the flatness of the neutral potential in this coordinate should lead to a long, anharmonic vibrational progression in this bending motion in the photoelectron spectrum. As a consequence of the large geometry changes upon photodetachment to the $\tilde{X}(^3B)$ state, standard normal-mode Franck−Condon simulations are not helpful in assigning the origin transition. Similarly, the calculated linear geometry of the $\tilde{b}(^1B)$ state should also produce a long progression in ∠CCH bending following photodetachment.

MRCI calculations predict a *cisoid*-bent geometry for the $\tilde{a}(^1A)$ state, with a nearly isoenergetic *transoid*-bent structure (Tables 2, S1). Each minimum on the $\tilde{a}(^1A)$ surface has ∠CCH similar to one of the anion states. Therefore, we expect good Franck−Condon overlap from each anion state with a minimum on the $\tilde{a}(^1A)$ surface.

6. DISCUSSION

6.1. Low-Lying Electronic States of HCCCH. The interpretation of the photoelectron spectrum of $HCCCH^-$ in the eBE = 1−3 eV range (Scheme 3) draws precedent from previous studies of HCCN,[68] HCNC,[68] and HCCCCN.[62] We assign the lowest energy electronic state of HCCCH as $\tilde{X}(^3B)$, with an experimental origin of 1.156 $\pm^{0.010}_{0.095}$ eV and a long vibrational progression indicative of a large geometry change compared to the anion. From the spectra, we estimate that the peak at 1.71 eV represents the maximum of the Franck−Condon envelope of the $\tilde{X}(^3B)$ state. By comparison, the CCSD(T) VDE from the $\tilde{X}(^2B)$ anion state is 1.77 eV, whereas the VDE from the $\tilde{A}(^2A)$ state (calculated to lie 0.026 eV above the $\tilde{X}$ state) is 1.70 eV. The decrease of 70 meV demonstrates the better Franck−Condon overlap of the $\tilde{A}(^2A)$ anion with the ground state neutral.

Scheme 3

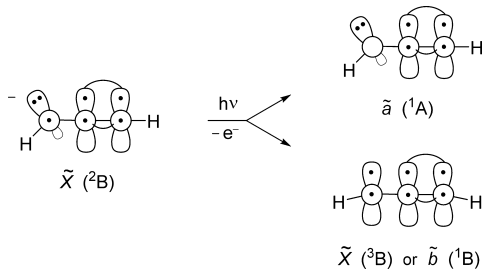

The sharp peak at eBE = 1.656 ± 0.005 eV, with β = −0.79, is consistent with the origin peak of the $\tilde{a}(^1A)$ state of HCCCH, providing a singlet−triplet splitting of ΔE_{ST} = 0.500 $\pm^{0.10}_{0.01}$eV. Noting the $\beta \sim -0.41$ value of the strong $\tilde{X}(^3B)$ peaks at 1.588 and 1.526 eV, we can use the more negative peaks of β(E) at higher binding energy to assign vibrational transitions belonging to the $\tilde{a}(^1A)$ state (vertical dashed lines in Figure 3a). The peak at 1.803 eV in Figure 3b is the only other peak that can be conclusively assigned to the $\tilde{a}(^1A)$ state. The energy of this peak is 0.147 ± 0.005 eV (1,186 ± 40 cm^{-1}) above the $\tilde{a}(^1A)$ origin, consistent with the totally symmetric CCC symmetric stretch vibration. The experimental spectra are consistent with a small geometry change from anion to neutral for the $\tilde{a}(^1A)$ electronic state.

An important constraint regarding the calculated energy gap between the $\tilde{X}(^2B)$ and $\tilde{A}(^2A)$ anion states can be derived from the experimental spectra. The calculated gap is 0.026 eV using CCSD(T)/CBS, and 0.014 eV using MRCI/CBS. Because our calculations of the neutral predict nearly isoenergetic *transoid*- and *cisoid*-bent geometries of the $\tilde{a}(^1A)$ state, *both* anion states should have nearly vertical transitions to the $\tilde{a}(^1A)$ state, yet we do not observe a splitting in the peak at 1.656 eBE. Although it is possible the two anion states differ in energy by our observed peak spacing of 0.147 eV, this explanation is unlikely because the population in the upper anion state would be low if it were 0.147 eV above the ground anion state. It therefore seems likely that the energy gap between the $\tilde{X}(^2B)$ and $\tilde{A}(^2A)$ anion states is less than the CCSD(T) calculated value of 0.026 eV. Because there is no experimentally observed splitting arising from the two predicted anion states, we consider only one anion state in our interpretation of transitions to all neutral states. This simplification may not be justified if higher resolution spectra become available in the future.

We assign the $\tilde{b}(^1B)$ state to the series of peaks from ∼2.4−2.95 eV with a band maximum of 2.65 ± 0.02 eV. We expect the geometry of the $\tilde{b}(^1B)$ state to be similar to the $\tilde{X}(^3B)$ state, because each arises upon removal of an electron (either α or β spin, respectively) from the same orbital of the anion. Similar to the $\tilde{X}(^3B)$ state, the $\tilde{b}(^1B)$ state exhibits a broad vibrational progression in the photoelectron spectrum (red spectra in Figure 3a and b). It is reasonable to expect that the energy gap between the band maxima and the ADEs will be similar given that the electronic structures of these two neutral states differ only in spin multiplicity. Using this energy difference from the $\tilde{X}(^3B)$ state ((1.71 − 1.156) = 0.554 eV), the origin of the $\tilde{b}(^1B)$ state is approximated as 2.65 − 0.554 ∼ 2.10 eV. However, the MRCI calculated VDE − ADE energy gap for the $\tilde{b}(^1B)$ state is 0.80 eV, much higher than the calculated or observed gap in the $\tilde{X}(^3B)$ state. This comparison suggests assigning an increased uncertainty to the purely experimental estimate of the origin energy in the $\tilde{b}(^1B)$ state as 2.10 ± 0.2 eV. Our experimental estimate of the term energy for the third electronic state of HCCCH is therefore T_0 [$\tilde{b}(^1B)$] = 0.94 $\pm^{0.22}_{0.20}$eV.

The measured energies of the lowest electronic states of propargylene **1** provide long-sought context for understanding the structure and chemical reactivity of this fundamentally important species. The singlet−triplet energy gap is a key parameter governing reactivity. When ΔE_{ST} is small (<2 kcal/mol), the spin states equilibrate rapidly in solution at room temperature, and the distinctive spin-state selectivity (stereo-

dx.doi.org/10.1021/ja5039984 | J. Am. Chem. Soc. XXXX, XXX, XXX−XXX

specific addition to alkenes by the singlet, nonstereospecific addition by the triplet) is lost.[74] The measured singlet−triplet energy gap of 11.5 kcal/mol for HCCCH is rather large and is consistent with the distinct reactivity observed for singlet and triplet states in solution.[74,75] Rate constants for intersystem crossing are not known, but the observation of stereospecific addition of the singlet to alkenes implies that bimolecular trapping of the highly reactive singlet carbene is faster than intersystem crossing to the triplet ground state. This situation is commonly observed in carbene chemistry.

These experiments also provide insight concerning the influence of an alkyne substituent on the singlet−triplet gap of a carbene. The simplest carbene, methylene (H_2C:), exhibits ΔE_{ST} = 9.09 kcal/mol.[53] It has long been appreciated that the introduction of a substituent with a π-electron system leads to a reduction in the magnitude of the singlet−triplet gap. In the case of phenyl carbene, the extra conjugation is considered to stabilize the singlet state more than the triplet state, leading to a smaller value of ΔE_{ST} = 5 kcal/mol. Qualitatively, one might anticipate a similar effect for propargylene, but our measurements reveal that this is not the case. Rather, the introduction of the ethynyl substituent increases ΔE_{ST} (11.5 kcal/mol) for HCCCH. The additional conjugation afforded by the ethynyl group undoubtedly stabilizes both singlet and triplet states, but it must be the case that the triplet state of HCCCH gains more stabilization than the singlet state. The effect is not large, and likely involves subtle factors involving electron exchange and electron correlation, some of which have been discussed previously in the context of the zero-field splitting parameters of triplet HCCCH.[1] The singlet−triplet splitting of HCCCH is very similar to that of the isoelectronic HC—C≡N (ΔE_{ST} = 0.510 eV, 11.8 kcal/mol),[62,68] but smaller than that of the more highly conjugated HC≡C—C—C≡N (ΔE_{ST} = 0.76 eV, 18 kcal/mol).[62]

6.2. Interpretation of Photoelectron Angular Distribution Measurements. The experimental angular distributions provide additional evidence on the orbital character of HCCCH and its anions. In atomic systems detachment from an *s* orbital ejects an electron as a pure *p*-wave (l = 1) and β = +2, independent of eKE. Detachment from an atomic *p*-orbital creates both *s* (l = 0; β = 0) and *d* (l = 2; β = −1) partial waves, which will interfere with each other to create anisotropy parameters between −1 and 0. At low eKE, *s*-waves dominate,[69] with *d*-waves dominating at eKE ∼ 1 eV.[70,71] Although it is only an approximation for molecules, we apply these qualitative concepts to the present case of HCCCH.

The experimental values of the anisotropy parameter upon detachment to different HCCCH electronic states are β [$\tilde{X}(^3B)$] ∼ −0.45, β [$\tilde{a}(^1A)$] ∼ −0.8, and β [$\tilde{b}(^1B)$] = −0.1 to +0.2 with increasing eBE (decreasing eKE). Detachment to the $\tilde{X}(^3B)$ state nominally corresponds to ejection of an electron from the β_{10} orbital (see Figures S6, S7 in the Supporting Information), which has mixed σ/π character in the bent anion. We thus expect β to be negative in sign but moderate in magnitude, consistent with the anisotropy parameter β = −0.45 observed for this state. Detachment to the $\tilde{a}(^1A)$ state nominally corresponds to ejection of an electron from the α_{11} orbital of nearly pure π symmetry, which is consistent with the observed very negative anisotropy parameter β = −0.8. Finally, the $\tilde{b}(^1B)$ state is formed by removal of the α_{10} electron. Because this orbital's shape is very similar to β_{10}, it should have a nearly identical mixture of π and σ character. In the $\tilde{b}(^1B)$ state, the observed anisotropy parameter ranges from β (eK*E* = 1.0 eV) = −0.1 to β (eK*E* = 0.46 eV) = +0.2. The smaller values of β at lower eKEs are again consistent with detachment from an orbital that has π character (a negative β component that decreases in magnitude as kinetic energy decreases) and σ character (contributing a positive β component independent of eKE). These orbital characters, in turn, are consistent with a nearly planar C_2 symmetry structure.

6.3. Higher Lying Electronic States of HCCCH. Assignments of the higher lying peaks from the VMI spectrometer (at eB*E* = 4.454, 4.590, 4.738, and 4.869 eV) are not as straightforward as in the NIPES spectra. Because of background signals inherent in these experiments, the angular distributions from the VMI apparatus are not quantitative, which removes a key observable in the assignment of electronic states. Nevertheless, on the basis of the intensities, it seems reasonable to assign the 4.454 eV peak as the origin of an electronic state. The MRCI results in Table 2, corrected for the 0.13 eV offset, predict ADEs of $\tilde{c}(^1\Sigma^+)$ = 2.61 eV, $\tilde{A}(^3B_2)$ = 4.39 eV, $\tilde{d}(^1A_2)$ = 4.42 eV, and $\tilde{B}(^3A_2)$ = 4.49 eV. The first two of these states have large geometry changes compared to the anion, which would make them difficult to observe, whereas the latter two states have small geometry changes. Inspection of the molecular orbitals of these states shows that all of them are accessible by removal of one electron from either anion state, in agreement with the propensity rule favoring single-electron transitions. Energetically, the best match with the 4.454 eV experimental origin peak is the $\tilde{d}(^1A_2)$ state, which has a small VDE-ADE gap, implying a fairly small geometry change from the anion, consistent with the VMI spectrum. The peak at 4.590 eV lies 0.136 eV (1097 cm^{-1}) above the origin, a value consistent with a CCC stretching mode, to which we tentatively assign it. However, the third peak is located 0.284 eV (2291 cm^{-1}) above the origin peak. It is difficult to rationalize this spacing as a vibrational fundamental or, based on the intensities, as a combination band built off the 4.454 eV origin peak. Therefore, it seems likely that the peak at 4.738 eV represents the origin of an additional electronic state with a similar geometry to the anion. We tentatively assign it as the $\tilde{B}(^3A_2)$ state, which is also characterized by a small geometry change from the anion. In the absence of additional experimental observables, it is difficult to determine more about these high-lying electronic states of HCCCH.

6.4. Vibrational Assignments in the $\tilde{X}(^3B)$ State of HCCCH. The vibrational peak spacings in the main progressions of the $\tilde{X}(^3B)$ state of HCCCH and DCCCD can be found in Table 1. On the basis of our assignment of the origin transition at eBE = 1.156 eV in the $\tilde{X}(^3B)$ state, the fundamental frequency of the main progression in HCCCH is 363 ± 57 cm^{-1}. Note that peak spacings in both isotopologues increase with increasing energy in the potential well. This "negative" anharmonicity arises from quartic terms in the 1-D vibrational potential and is indicative of a box-like potential arising from vibronic coupling. The shapes of the potentials in both the CCH and the CCC coordinates of the neutral $\tilde{X}(^3B)$ state (Figure S5) are consistent with negative anharmonicity.

The 363 ± 57 cm^{-1} fundamental frequency is difficult to reconcile with the known IR matrix spectrum of $\tilde{X}(^3B)$ propargylene,[3,32−34] where four bending mode bands are observed: 550 cm^{-1} (m), 403 cm^{-1} (m), 249 cm^{-1} (s), and 246 cm^{-1} (m). Matrix EPR data suggest that HCCCH undergoes motional averaging in various matrices, suggesting that the matrix is not imposing a structural constraint on the

dx.doi.org/10.1021/ja5039984 | J. Am. Chem. Soc. XXXX, XXX, XXX−XXX

molecule. The best assignment of the main progression we observe in HCCCH $\tilde{X}(^3B)$ is mode 4A, the "in-plane" symmetric CCH bend, with harmonic frequency ω_e(exp.) = 353 cm^{-1} (see Table S2), and ω_e(calc.) = 359 cm^{-1}. The calculated infrared harmonic intensity of 53 km/mol implies that this mode should also feature prominently in the IR spectrum, but there is no clear correspondence between the observed and calculated IR transition energies. We conclude that the quasilinear nature of HCCCH renders a harmonic, separable modes calculation substantially inadequate to compare with either the photoelectron or IR spectroscopy results. A detailed analysis will require a theoretical approach that includes anharmonicity, mode coupling, and vibronic coupling. The complexity of the problem is underscored by the fact that propargylene is a case that results from a strong Renner−Teller interaction at the nearby linear geometry and for which simple arguments based on the adiabatic potential energy surface may not be quantitatively reliable.[72,73]

CONCLUSIONS

The electronic and vibrational structure of propargylene (HCCCH) has been investigated using negative ion photoelectron spectroscopy and high-level electronic structure theory. Treatment of $CH_3C{\equiv}CH$ with O^- results in removal of a hydrogen atom and a proton to produce the $C_3H_2^-$ isomers $HCCCH^-$ and H_2CCC^- (m/z = 38). The negative ion photoelectron spectrum of $HCCCH^-$ yields spectroscopic and thermodynamic information concerning five electronic states of the corresponding neutral species, HCCCH.

Photodetachment of an electron from $HCCCH^-$ using near-UV radiation produces the $\tilde{X}(^3B)$ ground state of HCCCH and its $\tilde{a}(^1A)$, $\tilde{b}(^1B)$, $\tilde{d}(^1A_2)$, and $\tilde{B}(^3A_2)$ excited states. An extended vibrational progression in both the $\tilde{X}(^3B)$ ground state and the open-shell singlet $\tilde{b}(^1B)$ state arises as a consequence of a substantial change in geometry upon electron photodetachment. It is notoriously difficult to assign the spectroscopic origin in systems of this type. Both experiment and theory conclusively show the dominant vibrational motion activated upon photodetachment is CCH bending. Through comparison of the $HCCCH^-$ and $DCCCD^-$ photoelectron spectra, the EA of HCCCH is determined to be 1.156 $\pm^{0.010}_{0.095}$ eV, with a singlet−triplet splitting between the $\tilde{X}(^3B)$ and the $\tilde{a}(^1A)$ states of ΔE_{ST} = 0.500 $\pm^{0.10}_{0.01}$ eV.

The photoelectron spectra associated with the $\tilde{a}(^1A)$, $\tilde{d}(^1A_2)$, and $\tilde{B}(^3A_2)$ states are characterized by short vibrational progressions with a prominent origin peak, establishing that the geometries of the anion and the neutral are similar. The lack of a resolvable splitting in the origin transition to the $\tilde{a}(^1A)$ state implies that the energy difference between the calculated ground and first excited state of the HCCCH anion is less than the calculated splitting of 0.026 eV.

A higher resolution photoelectron spectrum of the $\tilde{X}(^3B)$ state would likely reveal much more complicated vibrational structure due to the quasilinear nature of HCCCH. In fact there are signs in our spectra that more than one vibrational mode contributes to this progression at high binding energies. A more sophisticated analysis awaits higher resolution spectroscopy.

ASSOCIATED CONTENT

Supporting Information

Experimental Methods; Anharmonic Fitting Approach to Determine Electron Affinity; Molecular Orbitals and Bending Potentials; Energy Ordering of the Lowest Three HCCCH Electronic States; Figure S1, Photoelectron spectra of the product anions from O^- with allene-d_4 and with propyne-d_4.; Figure S2, Differential cross sections of the product anions of the O^- + propyne reaction; Figure S3, Photoelectron spectra normalized to the differential cross section; Figure S4, Calculated equilibrium geometries of the lowest two $HCCCH^-$ and lowest three HCCCH electronic states; Figure S5, Unrelaxed bending potentials of HCCCH/$HCCCH^-$; Table S1, Calculated geometries and harmonic frequencies; Figure S6, Molecular orbital diagrams for $HCCCH^-$ $\tilde{X}(^2B)$; Figure S7, Molecular orbital diagrams for $HCCCH^-$ $\tilde{A}(^2A)$; Figure S8, Candidate origin transition energies; Table S2, Fitting results to determine the origin transition energy. Geometric coordinates and energies in Hartrees of all optimized structures are available upon request from the authors. This material is available free of charge via the Internet at http://pubs.acs.org.

AUTHOR INFORMATION

Corresponding Authors

dlosbor@sandia.gov
wcl@jila.colorado.edu

Present Addresses

[#]Intel Corporation, 2510 NW 229th Avenue, Hillsboro, Oregon 97124
[▽]Chemical and Materials Sciences Center, National Renewable Energy Laboratory, 15013 Denver West Parkway, Golden, Colorado 80401
[○]Department of Chemistry, University of Wisconsin-Madison, Madison, Wisconsin, 53706

Notes

The authors declare no competing financial interest.

ACKNOWLEDGMENTS

This article is dedicated to the memory of Professor Charles H. DePuy (1927-2013). D.L.O. gratefully acknowledges a JILA Visiting Fellowship during which this data was collected, and support by the Division of Chemical Sciences, Geosciences, and Biosciences, the Office of Basic Energy Sciences, the U.S. Department of Energy. Sandia is a multiprogram laboratory operated by Sandia Corporation, a Lockheed Martin Company, for the National Nuclear Security Administration under contract DE-AC04-94-AL85000. R.J.M. gratefully acknowledges a JILA Visiting Fellowship, as well as support from the U.S. National Science Foundation (CHE-1011959). J.F.S. gratefully acknowledges support from the Robert A. Welch Foundation (Grant F-1283). L.B.H. and B.R. gratefully acknowledge support by the U.S. Department of Energy, Office of Basic Energy Sciences, Division of Chemical Sciences, Geosciences, and Biosciences, under Contract No. DE-AC02-06CH11357. W.C.L. gratefully acknowledges support from NSF (PHY1125844 and CHE1213862) and AFOSR (FA9550-12-1-0125) for significant contributions to this project.

REFERENCES

(1) Seburg, R. A.; Patterson, E. V.; McMahon, R. J. *J. Am. Chem. Soc.* **2009**, *131*, 9442−9455.
(2) Seburg, R. A.; McMahon, R. J. *Angew. Chem., Int. Ed.* **1995**, *34*, 2009−2012.
(3) Seburg, R. A.; Patterson, E. V.; Stanton, J. F.; McMahon, R. J. *J. Am. Chem. Soc.* **1997**, *119*, 5847−5856.
(4) Matthews, H. E.; Irvine, W. M. *Astrophys. J.* **1985**, *298*, L61−L65.
(5) Thaddeus, P.; Vrtilek, J. M.; Gottlieb, C. A. *Astrophys. J.* **1985**, *299*, L63−l66.

dx.doi.org/10.1021/ja5039984 | *J. Am. Chem. Soc.* XXXX, XXX, XXX−XXX

(6) Madden, S. C.; Irvine, W. M.; Matthews, H. E.; Friberg, P.; Swade, D. A. *Astron. J.* **1989**, *97*, 1403−1422.
(7) Reisenauer, H. P.; Maier, G.; Riemann, A.; Hoffmann, R. W. *Angew. Chem., Int. Ed.* **1984**, *23*, 641.
(8) Bogey, M.; Demuynck, C.; Destombes, J. L.; Dubus, H. *J. Mol. Spectrosc.* **1987**, *122*, 313−324.
(9) Clauberg, H.; Minsek, D. W.; Chen, P. *J. Am. Chem. Soc.* **1992**, *114*, 99−107.
(10) Kanata, H.; Yamamoto, S.; Saito, S. *Chem. Phys. Lett.* **1987**, *140*, 221−224.
(11) Lovas, F. J.; Suenram, R. D.; Ogata, T.; Yamamoto, S. *Astrophys. J.* **1992**, *399*, 325−329.
(12) Cernicharo, J.; Gottlieb, C. A.; Guelin, M.; Killian, T. C.; Paubert, G.; Thaddeus, P.; Vrtilek, J. M. *Astrophys. J.* **1991**, *368*, L39−L41.
(13) Cernicharo, J.; Gottlieb, C. A.; Guelin, M.; Killian, T. C.; Thaddeus, P.; Vrtilek, J. M. *Astrophys. J.* **1991**, *368*, L43−L45.
(14) Cernicharo, J.; Cox, P.; Fosse, D.; Gusten, R. *Astron. Astrophys.* **1999**, *351*, 341−346.
(15) Maier, J. P.; Walker, G. A. H.; Bohlender, D. A.; Mazzotti, F. J.; Raghunandan, R.; Fulara, J.; Garkusha, I.; Nagy, A. *Astrophys. J.* **2011**, *726*, 41.
(16) Oka, T.; McCall, B. J. *Science* **2011**, *331*, 293−294.
(17) Liszt, H.; Sonnentrucker, P.; Cordiner, M.; Gerin, M. *Astrophys. J.* **2012**, *753*, L28.
(18) Vrtilek, J. M.; Gottlieb, C. A.; Gottlieb, E. W.; Killian, T. C.; Thaddeus, P. *Astrophys. J.* **1990**, *364*, L53−L56.
(19) McCarthy, M. C.; Thaddeus, P. *J. Mol. Spectrosc.* **2002**, *211*, 235−240.
(20) Gottlieb, C. A.; Killian, T. C.; Thaddeus, P.; Botschwina, P.; Flugge, J.; Oswald, M. *J. Chem. Phys.* **1993**, *98*, 4478−4485.
(21) Gauss, J.; Stanton, J. F. *J. Mol. Struct.* **1999**, *485*, 43−50.
(22) Maier, G.; Reisenauer, H. P.; Schwab, W.; Cársky, P.; Hess, B. A.; Schaad, L. J. *J. Am. Chem. Soc.* **1987**, *109*, 5183−5188.
(23) Oakes, J. M.; Ellison, G. B. *Tetrahedron* **1986**, *42*, 6263−6267.
(24) Robinson, M. S.; Polak, M. L.; Bierbaum, V. M.; DePuy, C. H.; Lineberger, W. C. *J. Am. Chem. Soc.* **1995**, *117*, 6766−6778.
(25) Stanton, J. F.; Garand, E.; Kim, J.; Yacovitch, T. I.; Hock, C.; Case, A. S.; Miller, E. M.; Lu, Y.-J.; Vogelhuber, K. M.; Wren, S. W.; Ichino, T. I.; Maier, J. P.; McMahon, R. J.; Osborn, D. L.; Neumark, D. M.; Lineberger, W. C. *J. Chem. Phys.* **2012**, *136* (134312), 1−16.
(26) Stanton, J. F.; DePinto, J. T.; Seburg, R. A.; Hodges, J. A.; McMahon, R. J. *J. Am. Chem. Soc.* **1997**, *119*, 429−430.
(27) Hodges, J. A.; McMahon, R. J.; Sattelmeyer, K. W.; Stanton, J. F. *Astrophys. J.* **2000**, *544*, 838−842.
(28) Tulej, M.; Guthe, F.; Pachkov, M. V.; Tikhomirov, K.; Xu, R.; Jungen, M.; Maier, J. P. *Phys. Chem. Chem. Phys.* **2001**, *3*, 4674−4678.
(29) Birza, P.; Chirokolava, A.; Araki, M.; Kolek, P.; Maier, J. P. *J. Mol. Spectrosc.* **2005**, *229*, 276−282.
(30) Achkasova, E.; Araki, M.; Denisov, A.; Maier, J. P. *J. Mol. Spectrosc.* **2006**, *237*, 70.
(31) Bernheim, R. A.; Kempf, R. J.; Gramas, J. V.; Skell, P. S. *J. Chem. Phys.* **1965**, *43*, 196−200.
(32) Chi, F. K. Ph.D. Thesis, Michigan State University, 1972.
(33) Jacox, M. E.; Milligan, D. E. *Chem. Phys.* **1974**, *4*, 45−61.
(34) Maier, G.; Reisenauer, H. P.; Schwab, W.; Carsky, P.; Spirko, V.; Hess, B. A.; Schaad, L. J. *J. Chem. Phys.* **1989**, *91*, 4763−4773.
(35) Seburg, R. A.; DePinto, J. T.; Patterson, E. V.; McMahon, R. J. *J. Am. Chem. Soc.* **1995**, *117*, 835−836.
(36) Miller, J. A.; Melius, C. F. *Combust. Flame* **1992**, *91*, 21−39.
(37) Miller, J. A.; Volponi, J. V.; Pauwels, J. F. *Combust. Flame* **1996**, *105*, 451−461.
(38) Bhargava, A.; Westmoreland, P. R. *Combust. Flame* **1998**, *113*, 333−347.
(39) Boullart, W.; Devriendt, K.; Borms, R.; Peeters, J. *J. Phys. Chem.* **1996**, *100*, 998−1007.
(40) Taatjes, C. A.; Klippenstein, S. J.; Hansen, N.; Miller, J. A.; Cool, T. A.; Wang, J.; Law, M. E.; Westmoreland, P. R. *Phys. Chem. Chem. Phys.* **2005**, *7*, 806−813.
(41) Maksyutenko, P.; Zhang, F. T.; Gu, X. B.; Kaiser, R. I. *Phys. Chem. Chem. Phys.* **2011**, *13*, 240−252.
(42) Vereecken, L.; Peeters, J. *J. Phys. Chem. A* **1999**, *103*, 5523−5533.
(43) Guadagnini, R.; Schatz, G. C.; Walch, S. P. *J. Phys. Chem. A* **1998**, *102*, 5857−5866.
(44) Nguyen, T. L.; Mebel, A. M.; Lin, S. H.; Kaiser, R. I. *J. Phys. Chem. A* **2001**, *105*, 11549−11559.
(45) Walch, S. P. *J. Chem. Phys.* **1995**, *103*, 7064−7071.
(46) Goulay, F.; Trevitt, A. J.; Meloni, G.; Selby, T. M.; Osborn, D. L.; Taatjes, C. A.; Vereecken, L.; Leone, S. R. *J. Am. Chem. Soc.* **2009**, *131*, 993−1005.
(47) Steinbauer, M.; Lang, M.; Fischer, I.; de Miranda, B. K. C.; Romanzin, C.; Alcaraz, C. *Phys. Chem. Chem. Phys.* **2011**, *13*, 17956−17959.
(48) Casey, C. P.; Kraft, S.; Powell, D. R. *J. Am. Chem. Soc.* **2000**, *122*, 3771−3772.
(49) Casey, C. P.; Boller, T. M.; Kraft, S.; Guzei, I. A. *J. Am. Chem. Soc.* **2002**, *124*, 13215−13221.
(50) Padwa, A.; Austin, D. J.; Gareau, Y.; Kassir, J. M.; Xu, S. L. *J. Am. Chem. Soc.* **1993**, *115*, 2637−2647.
(51) Hansen, E. C.; Lee, D. S. *Acc. Chem. Res.* **2006**, *39*, 509−519.
(52) Ervin, K. M.; Lineberger, W. C. In *Advances in Gas Phase Ion Chemistry*; Adams, N. G., Babcock, L. M., Eds.; JAI: Greenwich, 1992; Vol. *1*, pp 121−166.
(53) Leopold, D. G.; Murray, K. K.; Stevens Miller, A. E.; Lineberger, W. C. *J. Chem. Phys.* **1985**, *83*, 4849−4865.
(54) Ervin, K. M.; Ho, J.; Lineberger, W. C. *J. Chem. Phys.* **1989**, *91*, 5974−5992.
(55) Dawson, J. H. J.; Kaandorp, T. A. M.; Nibbering, N. M. M. *Org. Mass Spectrom.* **1977**, *12*, 330−333.
(56) Chandler, D. W.; Houston, P. L. *J. Chem. Phys.* **1987**, *87*, 1445−1447.
(57) Eppink, A.; Parker, D. H. *Rev. Sci. Instrum.* **1997**, *68*, 3477−3484.
(58) Sheps, L.; Miller, E. M.; Lineberger, W. C. *J. Chem. Phys.* **2009**, *131* (064304), 1−8.
(59) Aguilera-Iparraguirre, J.; Boese, A. D.; Klopper, W.; Ruscic, B. *Chem. Phys.* **2008**, *346*, 56−68.
(60) Frisch, M. J.; Trucks, G. W.; Schlegel, H. B.; Scuseria, G. E.; Robb, M. A.; Cheeseman, J. R.; Scalmani, G.; Barone, V.; Mennucci, B.; Petersson, G. A.; Nakatsuji, H.; Caricato, M.; Li, X.; Hratchian, H. P.; Izmaylov, A. F.; Bloino, J.; Zheng, G.; Sonnenberg, J. L.; Hada, M.; Ehara, M.; Toyota, K.; Fukuda, R.; Hasegawa, J.; Ishida, M.; Nakajima, T.; Honda, Y.; Kitao, O.; Nakai, H.; Vreven, T.; Montgomery, J., J. A.; Peralta, J. E.; Ogliaro, F.; Bearpark, M.; Heyd, J. J.; Brothers, E.; Kudin, K. N.; Staroverov, V. N.; Kobayashi, R.; Normand, J.; Raghavachari, K.; Rendell, A.; Burant, J. C.; Iyengar, S. S.; Tomasi, J.; Cossi, M.; Rega, N.; Millam, N. J.; Klene, M.; Knox, J. E.; Cross, J. B.; Bakken, V.; Adamo, C.; Jaramillo, J.; Gomperts, R.; Stratmann, R. E.; Yazyev, O.; Austin, A. J.; Cammi, R.; Pomelli, C.; Ochterski, J. W.; Martin, R. L.; Morokuma, K.; Zakrzewski, V. G.; Voth, G. A.; Salvador, P.; Dannenberg, J. J.; Dapprich, S.; Daniels, A. D.; Farkas, Ö.; Foresman, J. B.; Ortiz, J. V.; Cioslowski, J.; Fox, D. J. *Gaussian 09*, Revision A.1; Gaussian, Inc.: Wallingford, CT, 2009.
(61) Werner, H.-J.; Knowles, P. J.; Knizia, G.; Manby, F. R.; Schütz, M.; Celani, P.; Korona, T.; Lindh, R.; Mitrushenkov, A.; Rauhut, G.; Shamasundar, K. R.; Adler, T. B.; Amos, R. D.; Bernhardsson, A.; Berning, A.; Cooper, D. L.; Deegan, M. J. O.; Dobbyn, A. J.; Eckert, F.; Goll, E.; Hampel, C.; Hesselmann, A.; Hetzer, G.; Hrenar, T.; Jansen, G.; Köppl, C.; Liu, Y.; Lloyd, A. W.; Mata, R. A.; May, A. J.; McNicholas, S. J.; Meyer, W.; Mura, M. E.; Nicklass, A.; O'Neill, D. P.; Palmieri, P.; Pflüger, K.; Pitzer, R.; Reiher, M.; Shiozaki, T.; Stoll, H.; Stone, A. J.; Tarroni, R.; Thorsteinsson, T.; Wang, M.; Wolf, A. *MOLPRO*, version 2010.1, a package of ab initio programs (2010), see http://www.molpro.net.
(62) Vogelhuber, K. M.; Wren, S. W.; Shaffer, C. J.; McMahon, R. J.; McCoy, A. B.; Lineberger, W. C. *J. Chem. Phys.* **2011**, *135* (204307), 1−9.

(63) Taylor, T. R.; Bise, R. T.; Asmis, K. R.; Neumark, D. M. *Chem. Phys. Lett.* **1999**, *301*, 413−416.
(64) Ikuta, S. *J. Chem. Phys.* **1997**, *107*, 4579−4584.
(65) Vogelhuber, K. M.; Wren, S. W.; McCoy, A. B.; Ervin, K. M.; Lineberger, W. C. *J. Chem. Phys.* **2011**, *134* (184306), 1−13.
(66) Nee, M. J.; Osterwalder, A.; Zhou, J.; Neumark, D. M. *J. Chem. Phys.* **2006**, *125* (014306), 1−9.
(67) Peric, M.; Petkovic, M.; Jerosimic, S. *Chem. Phys.* **2008**, *343*, 141.
(68) Nimlos, M. R.; Davico, G.; Geise, C. M.; Wenthold, P. G.; Lineberger, W. C.; Blanksby, S. J.; Hadad, C. M.; Petersson, G. A.; Ellison, G. B. *J. Chem. Phys.* **2002**, *117*, 4323−4339.
(69) Wigner, E. P. *Phys. Rev.* **1948**, *73*, 1002−1009.
(70) Grumbling, E. R.; Sanov, A. *J. Chem. Phys.* **2011**, *135* (164302), 1−7.
(71) Hanstorp, D.; Bengtsson, C.; Larson, D. J. *Phys. Rev. A: At., Mol., Opt. Phys.* **1989**, *40*, 670−675.
(72) Stanton, J. F. *J. Chem. Phys.* **2010**, *133* (174309), 1−5.
(73) Simmons, C. S.; Ichino, T.; Stanton, J. F. *J. Phys. Chem. Lett.* **2012**, *3*, 1946−1950.
(74) Kirmse, W. *Carbene Chemistry*; 2nd ed.; Academic Press: New York, 1971; Chapter 8.
(75) Skell, P. S.; Klebe, J. *J. Am. Chem. Soc.* **1960**, *82*, 247−248.